GEOPHYSICS, VOL. 68, NO. 4 (JULY-AUGUST 2003); P. 1202–1210, 6 FIGS., 3 TABLES.
10.1190/1.1598112

New methods for shape and depth determinations from SP data

El-Sayed M. Abdelrahman*, Hesham M. El-Araby*, Abdel-Rady G. Hassaneen‡, and Mahfooz A. Hafez‡

ABSTRACT

We have extended our earlier derivative analysis method to higher derivatives to estimate the depth and shape (shape factor) of a buried structure from self-potential (SP) data. We show that numerical second, third, and fourth horizontal-derivative anomalies obtained from SP data using filters of successive window lengths can be used to simultaneously determine the depth and the shape of a buried structure. The depths and shapes obtained from the higher derivatives anomaly values can be used to determine simultaneously the actual depth and shape of the buried structure and the optimum order of the regional SP anomaly along the profile. The method is semi-automatic and it can be applied to residuals as well as to observed SP data.

We have also developed a method (based on a least-squares minimization approach) to determine, successively, the depth and the shape of a buried structure from the residual SP anomaly profile. By defining the zero anomaly distance and the anomaly value at the origin, the problem of depth determination has been transformed into the problem of finding a solution of a nonlinear equation of form $f(z) = 0$. Knowing the depth and applying the least-squares method, the shape factor is determined using a simple linear equation.

Finally, we apply these methods to theoretical data with and without random noise and on a known field example from Germany. In all cases, the depth and shape solutions obtained are in good agreement with the actual ones.

INTRODUCTION

One of the most important exploration problems is estimating the shape and depth of a buried structure. Different methods have been developed to determine the depth and the shape of the buried structure from self-potential (SP) data. The methods generally fall into one of the two categories. The first category includes 2D and 3D continuous modeling and inversion methods (Guptasarma, 1983; Furness, 1992; Shi and Morgan, 1996), which require current density and resistivity information as part of the input, along with some depth information obtained from geological and/or geophysical data. Thus, the resulting model can vary widely depending on these factors, but still give a calculated curve in close agreement with the observed data. The second category includes fixed simple geometry methods, in which the sphere, horizontal-cylinder, and vertical-cylinder models determine the depth and shape of the buried structure from residuals and/or observed SP data. The models may deviate from geological reality, but they are usually sufficient to determine whether the form and magnitude of the calculated SP effects are close enough to those observed to make the geological interpretation reasonable. The advantage of fixed geometry methods over 2D and 3D continuous modeling and inversion methods is that they do not require current density, resistivity, and depth information obtained from geological and/or geophysical data, and they can be applied if little or no factual information other than the SP data are available. For interpreting isolated simple source bodies, fixed geometry methods can be both fast and accurate.

Several methods have been developed to interpret SP data using a fixed simple geometry (Yungul, 1950; Meiser, 1962; Paul, 1965; Battacharya and Roy, 1981; Rao and Babu, 1983; Abdelrahman and Sharafeldin, 1997; and many others). However, most of these methods demand an a priori knowledge of the shape (shape factor) of the anomalous body, for example, whether the source is a sphere or a cylinder.

Few methods have been developed to determine the shape of the buried structure from a SP anomaly profile. These include, for example, the least-squares method (Abdelrahman et al., 1997a), numerical gradient method (Abdelrahman et al., 1997b), and derivative analysis method (Abdelrahman et al., 1998). In the present paper, we have extended the derivative analysis method (Abdelrahman et al., 1998) to higher

Manuscript received by the Editor January 31, 2001; revised manuscript received February 25, 2003.
*Cairo University, Geophysics Department, Faculty of Science, Giza, Egypt. E-mail: sayed5005@yahoo.com; hmaraby@hotmail.com.
‡National Research Institute of Astronomy and Geophysics, Helwan, Cairo, Egypt. E-mail: mahfoozh@hotmail.com.

derivatives to estimate the depth and shape of the source of a SP anomaly profile. We show that numerical second-, third-, and fourth-derivative anomalies obtained from observed SP data using filters of successive window lengths can be used to simultaneously determine the depth and shape of the buried structure and the optimum polynomial order for representing the regional SP anomaly. The method is superior to other published fixed geometry methods because it involves using simple models convolved with the same second, third, or fourth horizontal-derivative filter as applied to the observed SP data.

We have also developed a method (based on a least-squares minimization approach) to determine, successively, the depth and the shape of a buried structure from the residual SP anomaly profile. The least-squares method presented here can be applied when an individual SP anomaly is found that stands out so clearly that it can be separated from the regional background, and is so simple in appearance that it can be modeled as a single polarized body.

Finally, the validity of the methods is tested on a theoretical example with and without random noise and on a field example from Germany.

HIGHER DERIVATIVES ANALYSIS METHOD

Following Abdelrahman et al. (1998), the general expression for SP anomaly produced by some simple polarized geologic structure can be represented by the following equation:

$$V(x_i, z, \theta, q) = K\frac{x_i\cos\theta + z\sin\theta}{\left(x_i^2 + z^2\right)^q}, \qquad i = 1, 2, \ldots, N \tag{1}$$

where z is the depth, θ is the angle of polarization, K is the electric dipole moment, x_i is the position coordinate, and q is a factor related to the shape of the buried structure and is equal to 0.5, 1.0, and 1.5 for the semi-infinite vertical cylinder, horizontal cylinder, the sphere, respectively. The limits of applicability of equation (1) are described in Yungul (1950)

Let us consider five observation points ($x_i - 2s$, $x_i - s$, x_i, $x_i + s$, $x_i + 2s$) along the anomaly profile where $s = 1, 2, 3, \ldots, M$ spacing units is called the window length or graticule spacing. Using equation (1), the horizontal gradient of SP (dV/dx) using a central difference formula is given by

$$V_x(x_i, z, \theta, s) = \frac{K}{2s}\left\{\frac{(x_i + s)\cos\theta + z\sin\theta}{\left[(x_i + s)^2 + z^2\right]^q} - \frac{(x_i - s)\cos\theta + z\sin\theta}{\left[(x_i - s)^2 + z^2\right]^q}\right\}. \tag{2}$$

The second horizontal derivative SP anomaly is obtained from equation (2) as

$$V_{xx}(x_i, z, \theta, s) = \frac{K}{4s^2}\left\{\frac{(x_i + 2s)\cos\theta + z\sin\theta}{\left[(x_i + 2s)^2 + z^2\right]^q} - \frac{2x_i\cos\theta + 2z\sin\theta}{(x_i^2 + z^2)^q} + \frac{(x_i - 2s)\cos\theta + z\sin\theta}{\left[(x_i - 2s)^2 + z^2\right]^q}\right\}. \tag{3}$$

Using the value of V_{xx} at $x_i = 0$, equation (3) can be written as

$$V_{xx}(x_i, z, \theta, s) = \frac{V_{xx}(0)}{2z\sin\theta}\left[\frac{z^{2q}(4s^2 + z^2)^q}{z^{2q} - (4s^2 + z^2)^q}\right] \times \left\{\frac{(x_i + 2s)\cos\theta + z\sin\theta}{\left[(x_i + 2s)^2 + z^2\right]^q} - \frac{2x_i\cos\theta + 2z\sin\theta}{\left(x_i^2 + z^2\right)^q} + \frac{(x_i - 2s)\cos\theta + z\sin\theta}{\left[(x_i - 2s)^2 + z^2\right]^q}\right\}. \tag{4}$$

The numerical derivative values of equation (4) at $x_i = s$ and $x_i = -s$ are added (Abdelrahman et al., 1998) to obtain the following nonlinear equation:

$$d_{2i} - f_2(z, q, s_i) = 0, \qquad i = 1, 2, 3, \ldots, L \tag{5}$$

where $f_2(z, q, s_i)$ is a nonlinear function defined by

$$f_2(z, q, s_i) = \frac{z^{2q}(4s^2 + z^2)^q[(s^2 + z^2)^q - (9s^2 + z^2)^q]}{(s^2 + z^2)^q(9s^2 + z^2)^q[z^{2q} - (4s^2 + z^2)^q]},$$

and where

$$d_{2i} = \frac{V_{xx}(s) + V_{xx}(-s)}{V_{xx}(0)}.$$

For each value of q, equation (5) is solved for the depth (z) using the Newton-Raphson method (Demodivich and Maron, 1973). For a fixed window length, the computed depths are plotted against the shape factor representing continuous window curves. The solution of the depth and shape is read at the common intersection of the window curves. Theoretically, any two curves associated with two different values of s are enough to simultaneously determine z and q. In practice, more than two values of s are desirable because of the presence of noise in data.

Following the same approach used to derive equation (5), we obtain the nonlinear functions $f_3(z, q, s_i)$ and $f_4(z, q, s_i)$ for the third and the fourth derivative methods, respectively, as

$$f_3(z, q, s_i) = \frac{4[(s^2 + z^2)^q(9s^2 + z^2)^q][(4s^2 + z^2)^q - (16s^2 + z^2)^q]}{3[(4s^2 + z^2)^q(16s^2 + z^2)^q][(s^2 + z^2)^q - (9s^2 + z^2)^q]}, \tag{6}$$

and

$$f_4(z, q, s_i) = \left\{\frac{z^{2q}[(s^2 + z^2)^q(9s^2 + z^2)^q - 3(s^2 + z^2)^q(25s^2 + z^2)^q + 2(9s^2 + z^2)^q(25s^2 + z^2)^q]}{[z^{2q}(4s^2 + z^2)^q + 3(4s^2 + z^2)^q(16s^2 + z^2)^q - 4z^{2q}(16s^2 + z^2)^q]}\frac{(4s^2 + z^2)^q(16s^2 + z^2)^q}{(s^2 + z^2)^q(9s^2 + z^2)^q(25s^2 + z^2)^q}\right\}. \tag{7}$$

The d_i values for the third- and fourth-derivative methods are similar to those for second derivatives, except that V_{xx} is replaced by V_{xxx}, and V_{xxxx}, respectively.

In all cases, the numerical values of the derivative anomalies are computed from the observed data $V(x_i)$ from the following equations:

$$V_{xx}(x_i) = \frac{V(x_i + 2s) - 2V(x_i) + V(x_i - 2s)}{4s^2}, \qquad (8)$$

for the second-derivative anomalies,

$$V_{xxx}(x_i) = \frac{V(x_i + 3s) - 3V(x_i + s) + 3V(x_i - s) - V(x_i - 3s)}{8s^3}, \qquad (9)$$

for the third-derivative anomalies, and

$$V_{xxxx}(x_i) = \frac{V(x_i + 4s) - 4V(x_i + 2s) + 6V(x_i) - 4V(x_i - 2s) + V(x_i - 4s)}{16s^4}, \qquad (10)$$

for the fourth-derivative anomalies.

Note that real data contain measement errors, which may be compounded by errors in generating the window curves when using higher derivative anomalies. In spite of this, high structural resolution may be achieved at the expense of decreased tolerance to instrument reading errors. However, since the interpretation requires only a relatively short length of profile, the problem may be effectively overcome by increasing the number of measurements made within the restricted length of profile. The smoothed data may then be interpreted uniquely and precisely in terms of the assumed structure. At the same time, using a relatively short length of profile results in a very high rejection of the neighboring disturbances.

However, the accuracy of the results obtained using the above methods depends upon the accuracy to which the order of the polynomial representing the regional SP anomaly can be determined from the measured data.

OPTIMUM-ORDER REGIONAL DETERMINATION

Geologic interpretation of geophysical data invariably involves isolation of the geophysical anomaly in the presence of unwanted (or regional) data. Interpretation usually requires subtracting the estimated regional effect from the observed profile. However, serious distortions in the magnitude and extension of residual SP anomalies result from methods such as those defined by Peters (1949), Syberg (1972), Agarwal and Lal (1971), and Abdelrahman et al. (1985). The conclusion is inescapable that the resulting residuals (or derivatives) cannot yield a reliable geologic interpretation (Hammer, 1977). The argument probably applies in all forms of data processing, even processing in the frequency domain (Nettleton, 1976). If, however, the observed SP profile can be considered as the combined effect of a residual component due to a purely local structure and a regional component of any order p, then it is possible to formulate procedures to determine the optimum order of the regional SP anomaly along the profile and to obtain a true geologic interpretation.

The shapes and the depths of the buried structure computed from the different derivative anomalies can be used to determine the optimum order of the regional anomaly and to estimate the actual shape and depth of the buried structure. The procedure depends on the fact that the p-order derivative removes the effect of $p - 1$ order (and less) regional anomaly. The following cases are given for illustration.

Case 1.—If the shapes and depths (q_2, z_2), (q_3, z_3) of the buried structure computed from the second- and third-derivative anomalies are equal, then the regional anomaly can be represented by a zero- or first-order polynomial, and the true shape and depth are q_2 and z_2 (or q_3 and z_3). This is true because both second- and third-derivative operations remove the zero- or first-order regional SP anomaly from the data.

Case 2.—If $q_2 \neq q_3$ and $z_2 \neq z_3$ but $q_3 = q_4$ and $z_3 = z_4$, where q_4 and z_4 are computed from the fourth-derivative anomalies, the optimum-order of the regional anomaly can be represented by a second-order polynomial, and the true shape and depth are q_3 and z_3 (or q_4 and z_4). In this case, the second-derivative anomalies are generally distorted by the unremoved second-order regional anomaly, and consequently, the depth and the shape computed from the second-derivative anomalies are highly erroneous.

The above procedure is easily generalized in case of using fifth and/or higher derivative anomalies .

LEAST-SQUARES METHOD

Here, we have chosen the least-squares method to find the depth and the shape parameters of simple geometrical bodies from residual SP anomalies. This is because of its mathematical robustness when the recorded data are, in the words of Jackson (1972), "inaccurate, insufficient, and inconsistent."

For all shapes (function of q), equation (1) gives the following relationship at the origin ($x_i = 0$):

$$K = \frac{V(0) z^{2q-1}}{\sin\theta}, \qquad \sin\theta \neq 0, \qquad (11)$$

where $V(0)$ is the anomaly value at the origin.

Setting equation (1) to zero, we obtain the following equation:

$$\cot\theta = \frac{-z}{x_0}, \qquad (12)$$

where x_0 is the zero anomaly distance.

Using equations (11) and (12), equation (1) can be written in a normalized form as

$$\frac{x_0 V(x_i, z, q)}{V(0)(x_0 - x_i)} = \frac{z^{2q}}{(x_i^2 + z^2)^q}, \qquad x_i \neq x_0. \qquad (13)$$

In this way, we are able to eliminate K and θ from equation (1) by introducing two pieces of information, namely $V(0)$ and x_0.

Taking the logarithm of both sides of equation (13), we obtain

$$R(x_i, z, q) = \ln\left[\frac{x_0 V(x_i, z, q)}{V(0)(x_0 - x_i)}\right] = q \ln \frac{z^2}{x_i^2 + z^2}, \quad (14)$$

where $R(x_i, z, q)$ represents the logarithm of the normalized residual anomaly.

Again, for all shapes, equation (14) gives the following value at $x_i = a$:

$$R(a) = q \ln \frac{z^2}{a^2 + z^2}, \; a \neq 0. \quad (15)$$

Using equations (14) and (15), we obtain the following nonlinear equation in the depth (z):

$$R(x_i, z) = R(a) W(x_i, z), \quad (16)$$

where

$$W(x_i, z) = \frac{\ln \dfrac{z^2}{x_i^2 + z^2}}{\ln \dfrac{z^2}{a^2 + z^2}}.$$

Consequently the shape factor (q) is eliminated from equation (14) by introducing $R(a)$, that is, the potential at any point (a) on the x-axis other than zero.

The unknown depth (z) in equation (16) can be obtained by minimizing

$$\varphi(z) = \sum_{i=1}^{N} [L(x_i) - R(a) W(x_i, z)]^2, \quad (17)$$

where $L(x_i)$ denotes the logarithm of the normalized observed SP anomaly at x_i as shown in equation (14).

Setting the derivative of $\phi(z)$ with respect to z to zero leads to the following nonlinear equation in z:

$$f(z) = \sum_{i=1}^{N} [L(x_i) - R(a) W(x_i, z)] W^*(x_i, z) = 0, \quad (18)$$

where

$$W^*(x_i, z) = \frac{d(W(x_i, z))}{dz}.$$

Equations (18) can be solved for z using standard methods for solving nonlinear equation. Here, it is solved by an iteration method (Demidovich and Maron, 1973).

Substituting the computed depth (z_c) as a fixed parameter in equation (14), we obtain

$$R(x_i, q) = q \ln \frac{z_c^2}{x_i^2 + z_c^2}, \quad (19)$$

The unknown shape factor (q) in equation (19) can be obtained by minimizing

$$\psi(q) = \sum_{i=1}^{N} [L(x_i) - R(x_i, q)]^2, \quad (20)$$

where $L(x_i)$ denotes the logarithm of the normalized residual SP anomaly at x_i as shown in equation (14).

Setting the derivative of $\psi(q)$ with respect to q to zero leads to the following linear equation after simplification:

$$q_c = \frac{\sum_{i=1}^{N} L(x_i) \ln \dfrac{z_c^2}{x_i^2 + z_c^2}}{\sum_{i=1}^{N} \left[\ln \dfrac{z_c^2}{x_i^2 + z_c^2}\right]^2}. \quad (21)$$

Once z_c and q_c are known, the polarization angle θ can be determined from equation (12). Knowing θ, the electric dipole moment K can be determined from equation (11).

Finally, we measure the goodness of fit between the observed and the computed SP data for each (a) value. The most common way to compare two SP anomaly profiles is to compute the root-mean-square (rms) error between the observed values and values computed from the estimated parameters z, q, θ, and K. The model parameters which give the least sum squared differences are the best. In this way, we were able to select the most appropriate source parameter solutions.

We feel our approach is more advantageous than any least-squares inversion technique in determining the model parameters of the buried structures from a residual SP anomaly because it does not try to simultaneously solve for all unknowns. Rather it begins by solving for two parameters. The other parameters are then solved for in simple order. The optimization problem for obtaining the depth, shape, polarization angle, and dipole moment simultaneously is highly nonlinear.

The advantage of the present least-squares method over the higher derivatives analysis method presented earlier is that the depth and shape parameters can be computed from all observed residual data points. However, we recommend use of the higher derivatives analysis method when $V(0)$ and x_0 are difficult to determine from SP data due to the presence of regional components in the data.

Up to this stage, we have assumed knowledge of the origin when applying the higher derivatives and least-squares methods. In practice, a field traverse will have an arbitrary origin, in which case the position of the structure ($x_i = 0$) in equation (1) must first be determined. In most cases, the maximum and minimum values of the profile can be used to determine the correct location $x_i = 0$. A straight line joining the maximum to minimum of the profile will intersect the anomaly curve at the point $x_i = 0$ (Stanley, 1977).

SYNTHETIC EXAMPLE

We compute a theoretical SP anomaly of a horizontal cylinder ($q = 1, z = 3$ m, $K = -600$ mV, and $\theta = 40^\circ$) at 51 points with spacing of 1 m (Figure 1). The anomaly profile is subjected to separation techniques using the numerical derivative methods. Four successive second-, third- and fourth-derivative windows ($s = 2, 3, 4$, and 5 m) were applied to each set of input data. The methods are then applied to obtain the window curves from the numerical second-, third- and fourth-derivative anomalies, respectively. The results are shown in Figure 2 and summarized in Table 1.

The correct solution for the theoretical horizontal-cylinder model occurs at the common intersection of the window curves in case of using second-, third-, and fourth-derivative methods.

Figure 2 shows the intersection at the correct location $q = 1$ and $z = 3$ m.

Next, random errors of 5% were added to the SP anomaly to simulate noisy data. Four successive second-, third-, and fourth-derivative windows ($s = 2$, 3, 4, and 5 m) were then applied to the data. In this way, four sets of noisy second-, third- and fourth-derivative anomaly profiles were obtained from the SP anomaly profile. Adapting the same interpretation technique described above, the results are shown in Figure 3 and summarized in Table 1.

When the data are noisy, the window curve intersections are subject to interpretation. In the case of the noisy theoretical SP anomaly, the window curves generated from second-derivative anomalies intersect each other in a narrow region where $0.75 > q_2 > 1.2$ and 3.6 m $> z_2 >$ 2.7 m (Figure 3a). The central point of this intersection (intersection point) occurs at approximate location $z_2 = 3.05$ m and $q_2 = 0.96$. The window curves generated from the third-derivative anomalies intersect each other at $q_3 = 1.04$ and $z_3 = 3.2$ m (Figure 3b). Figure 3c shows that the window curves generated from the fourth-derivative anomalies intersect each other in a narrow region where $1.2 > q_4 > 0.7$ and 2.6 m $> z_4 >$ 3.6 m. The central point of this intersection occurs at the approximate location $q_4 = 0.94$ and $z_4 = 3.05$ m (Table 1). Thus, values of the shape and depth obtained from second-, third-, and fourth-derivative anomalies obtained from the noisy theoretical SP anomaly are

Table 1. Numerical results for computed shape and depth obtained from the synthetic example using the higher derivatives method.

	Second-derivative method	Third-derivative method	Fourth-derivative method
Using data	$q_2 = 1.0$	$q_3 = 1.0$	$q_4 = 1.0$
Without errors	$z_2 = 3.0$	$z_3 = 3.0$	$z_4 = 3.0$
Using data with	$q_2 = 0.96$	$q_3 = 1.04$	$q_4 = 0.94$
5% random errors	$z_2 = 3.05$	$z_3 = 3.20$	$z_4 = 3.05$

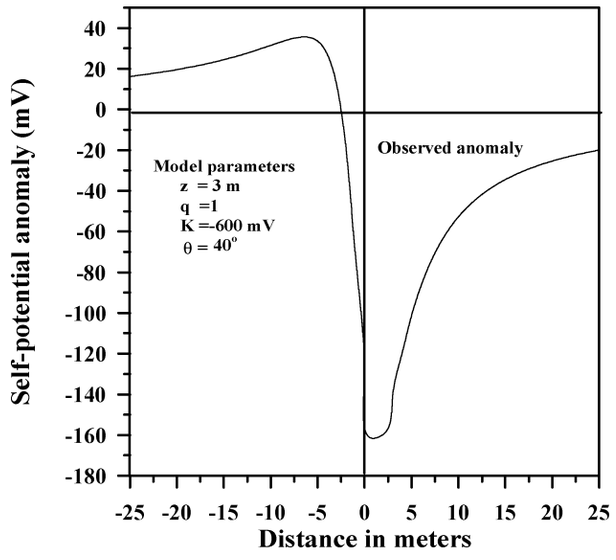

FIG. 1. A typical self-potential anomaly profile over a horizontal cylinder model.

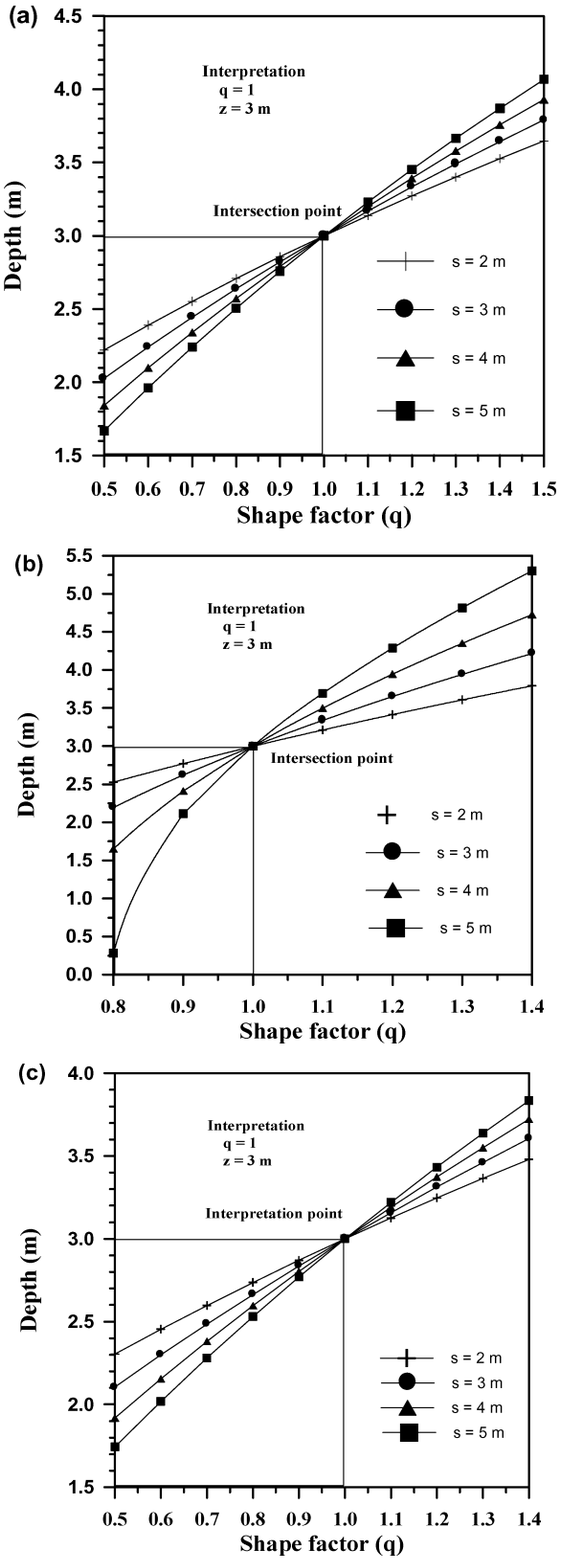

FIG. 2. Family of window curves of z as a function of q for $s = 2$, 3, 4, and 5 m using the present approach as obtained from noise free SP anomalies. Data interpretation of Figure 1 using (a) second-derivative method, (b) third-derivative method, and (c) fourth-derivative method.

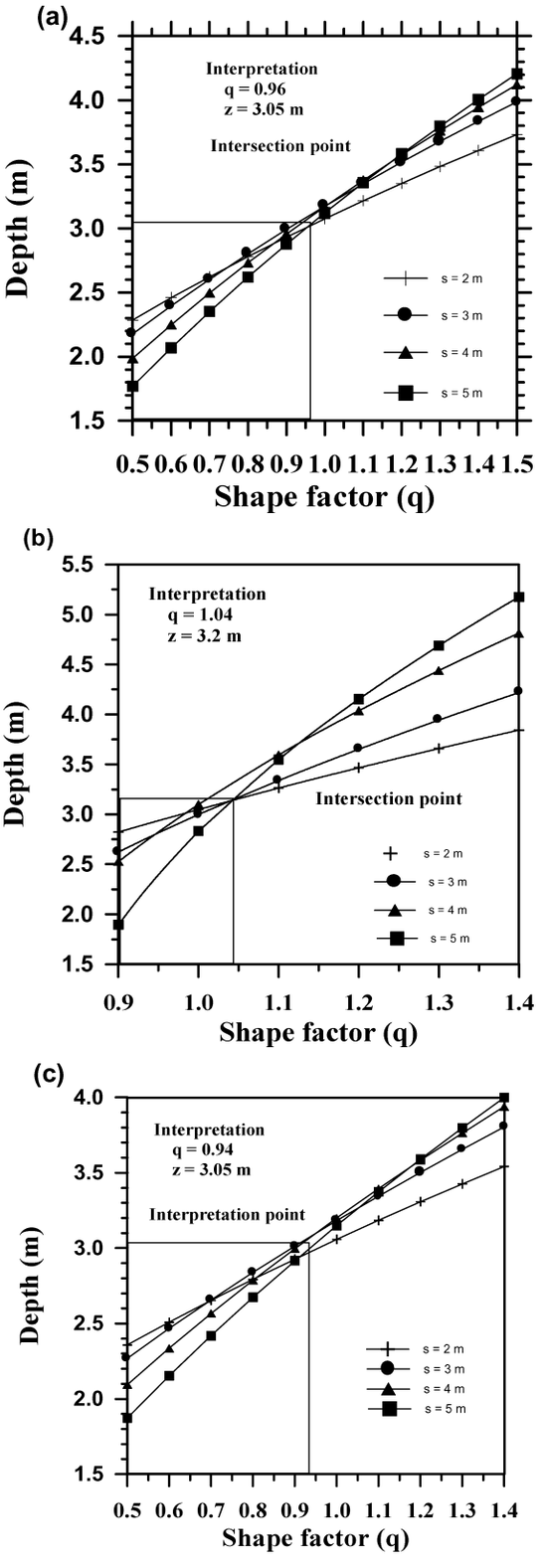

FIG. 3. Family of window curves of z as a function of q for $s = 2, 3, 4$, and 5 m using the present approach as obtained from noisy SP anomalies. Data interpretation of Figure 1 using (a) second-derivative method, (b) third-derivative method, and (c) fourth-derivative method.

in excellent agreement with the actual ones even when the data contain errors.

On the other hand, we have also applied the present least-squares method to the same noisy SP data of the theoretical horizontal-cylinder model . Equations (18), (21), (12), and (11) were used to determine the depth, the shape factor, the polariztion angle, and the electric dipole moment, respectively, using all possible cases of (a) values. The results are shown in Table 2. The best-fit model parameter are $z = 2.99$ m, $q = 0.996$, $\theta = 39.97°$, and $K = -603.7$ mV. The model parameters thus obtained from the present least-squares method are also in excellent agreement with the actual parameters ($z = 3$ m, $q = 1$, $\theta = 40°$, and $K = -600$ mV).

FIELD EXAMPLE

Figure 4 shows the SP anomaly over a graphite deposit in the southern Bavarian woods, Germany. The SP measurements were performed and described by Meiser (1962). This anomaly profile of 520-m length (Figure 4) was digitized at an interval of 10.41 m. Separation techniques were applied to the digitized values using the different derivative methods. Four successive derivative windows ($s = 20.82$, 31.23, 41.64, and 52.05 m) were applied (Figure 5). The second, third, and fourth derivatives thus obtained were used to generate the window curves shown in Figure 6. The results are summarized as follows:

$$q_2 = 0.79 \qquad z_2 = 43 \text{ m},$$
$$q_3 = 0.9 \qquad z_3 = 53 \text{ m},$$
$$q_4 = 1.05 \qquad z_4 = 51 \text{ m}.$$

Since $q_2 \neq q_3 \approx q_4$ and $z_2 \neq z_3 \approx z_4$, then the regional anomaly along the measured SP profile can be represented by a second-order polynomial. Also, the shape factor and the depth obtained by the higher derivatives method are $q = 0.9$ and $z = 53$ m, respectively. This suggests that the shape of the buried structure resembles a 2D horizontal-cylinder model buried at a depth of 53 m.

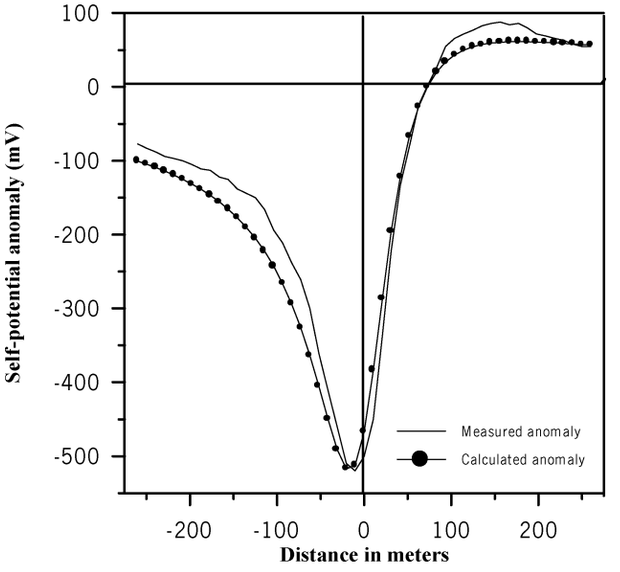

FIG. 4. Measured and calculated SP anomaly over a graphite ore body, southern Bavarian woods, Germany (after Meiser, 1962).

On the other hand, the least-squares method was also applied to the same anomaly profile of the field example to determine the model parameters of the buried structure. The values of $V(0)$ and x_0 usd in the least-squres method were -500 mV and 72 m (Figure 4) respectively, using the centeral (a) values on the profile. Then we computed the root-mean-square error (rms) between the observed values and the values computed from estimated parameters z, q, θ, and K. The results are shown in Table 3. The best-fit model parameters are $z = 49.3$ m, $q = .91$, $\theta = -55.7^\circ$ and $K = 2020$ mV. The shape factor thus obtained by the least-squares method suggests also that the shape of the 2D source body can be represented by a horizontal cylinder buried at a depth of 49.3 m. The depth obtained by the present higher derivatives and least-squares methods agrees with the depth (53 m) obtained by Meiser (1962) using a double logarithmic net method.

CONCLUSIONS

In this paper, we have improved our earlier derivative analysis method to higher derivatives for determining the depth and shape of a buried structure from SP data. We have shown that numerical higher derivative SP anomalies are useful tools for quantitative studies of SP data. Determining the depth, shape, and optimum regional anomaly order is possible. The method uses a simple model (sphere or cylinder) convolved with the

Table 2. Percentage of error in model parameters of the synthetic example in case of using the present least-squares method (best a value and minimum rms value in bold).

a (m)	Percent error in z	Percent error in q	Percent error in θ	Percent error in K	rms (mV)	a (m)	Percent error in z	Percent error in q	Percent error in θ	Percent error in K	rms (mV)
−25	0.538	2.738	0.471	−0.419	0.499	1	−18.56	−42.05	−10.58	22.24	8.101
−24	−0.0322	0.895	0.142	0.194	0.305	2	4.084	15.08	2.5146	−4.135	2.070
−23	0.338	2.090	0.356	−0.205	0.423	3	0.467	2.507	0.430	−0.343	0.471
−22	0.334	2.074	0.353	−0.200	0.421	4	1.536	6.050	1.046	−1.480	0.921
−21	0.323	2.040	0.347	−0.188	0.417	5	−1.817	−4.612	−0.88	2.135	0.692
−20	0.489	2.577	0.443	−0.366	0.479	6	1.459	5.790	1.002	−1.398	0.887
−19	−0.005.5	0.983	0.157	0.164	0.312	7	−0.955	−1.995	−0.389	1.192	0.358
−18	**−0.424**	**−0.345**	**−0.0836**	**0.616**	**0.255**	8	0.263	1.846	0.313	−0.124	0.396
−17	−0.299	0.0490	−001.12	0.481	0.259	9	0.329	2.060	0.351	−0.195	0.420
−16	1.002	4.264	0.739	−0.914	0.690	10	0.392	2.264	0.387	−0.262	0.443
−15	−0.103	0.672	0.101	0.269	0.289	11	0.562	2.817	0.485	−0.445	0.508
−14	−0.693	−1.187	−0.238	0.908	0.287	12	0.419	2.352	0.403	−0.292	0.453
−13	0.548	2.769	0.477	−0.429	0.502	13	−0.253	0.193	0.014	0.432	0.264
−12	−0.0980	0.688	0.104	0.264	0.290	14	0.196	1.630	0.274	−0.054	0.373
−11	−0.364	−0.156	−0.0490	0.552	0.258	15	−0.926	−1.908	−0.372	1.160	0.349
−10	−0.743	−1.341	−0.267	0.962	0.298	16	0.281	1.903	0.323	−0.143	0.402
−9	−0.781	−1.461	−0.289	1.004	0.308	17	0.241	1.776	0.300	−0.101	0.389
−8	0.163	1.524	0.255	−0.0169	0.362	18	0.461	2.486	0.426	−0.336	0.469
−7	−1.672	−4.181	−0.807	1.976	0.631	19	0.118	1.380	0.229	0.03102	0.348
−6	0.937	4.047	0.701	−0.844	0.662	20	−0.599	−0.892	−0.184	0.806	0.270
−5	0.505	2.631	0.452	−0.384	0.486	21	0.059	1.190	0.195	0.09484	0.330
−4	−0.518	−0.641	−0.137	0.718	0.260	22	0.370	2.191	0.374	−0.238	0.434
−3	−0.659	−1.079	−0.218	0.870	0.280	23	−0.0895	0.715	0.109	0.255	0.292
−2	3.698	13.65	2.2925	−3.738	1.894	24	−0.213	0.320	0.0379	0.389	0.269
−1	−17.60	−40.47	−10.02	21.00	7.682	25	−0.0165	0.947	0.151	0.176	0.309

Table 3. Numerical results of the present least-squares method applied to the field example (best fit in bold).

a (m)	Depth Z_c (m)	Shape factor q_c	Polarization angle θ_c (degree)	Electric dipole moment k_c (mV)	rms (mV)
−104.1	36.3	0.74	−65.4	930.3	27.7
−93.69	35.1	0.73	−66.2	878.8	28.6
−83.28	36.0	0.74	−65.5	918.5	27.9
−72.87	34.9	0.73	−66.4	870.2	28.8
−62.46	36.3	0.74	−65.3	935.4	27.6
−52.05	40.8	0.80	−61.9	1191.8	25.9
−41.64	41.6	0.81	−61.3	1255.8	25.9
−31.23	42.3	0.82	−60.8	1304.7	26.0
−20.82	**49.3**	**0.91**	**−55.7**	**2020.0**	**25.3**
10.41	19.4	0.52	−77.9	486.7	55.1
31.23	94.2	1.56	−31.5	96555.1	95.5
41.64	66.1	1.14	−44.8	7040.2	52.8
52.05	79.5	1.33	−37.7	22790.5	73.3
62.46	47.2	0.88	−57.2	1760.2	28.4
72.87	65.4	1.13	−45.2	6671.9	51.8
83.28	78.1	1.31	−38.4	19882.8	71.13
93.69	116.2	1.94	−24.6	1156551.0	127.3
104.1	103.9	1.72	−28.1	273950.4	109.7

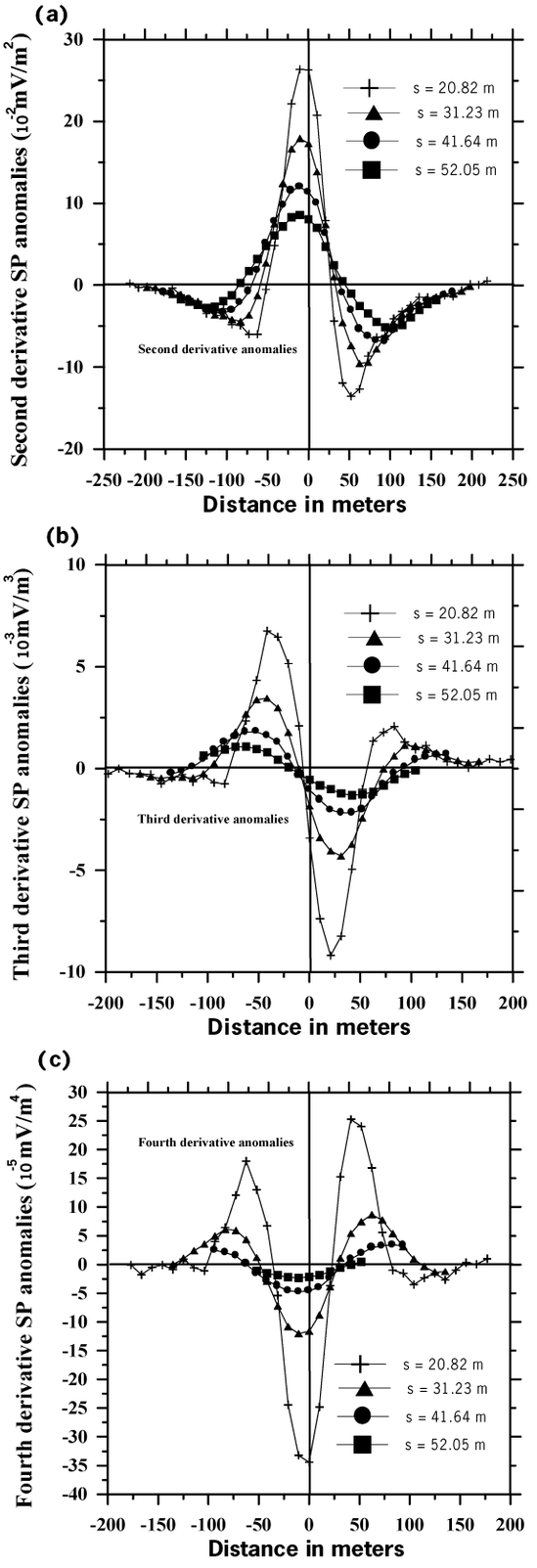

FIG. 5. Data analysis of measured SP anomaly over a graphite ore body, southern Bavarian woods, Germany, for $s = 20.82$, 31.23, 41.64, and 52.50 m using (a) second-derivative method, (b) third-derivative method, (c) fourth-derivative method.

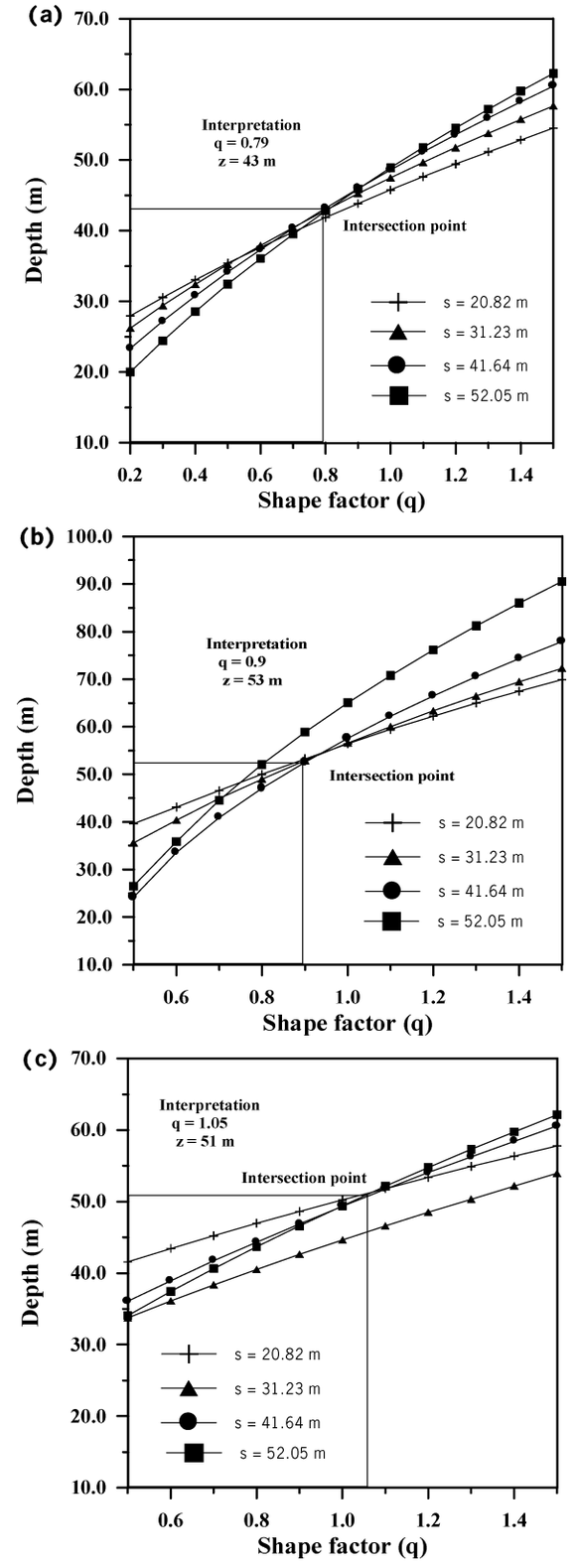

FIG. 6. Family of window curves of z as a function of q for $s = 20.82$, 31.23, 41.64, and 52.50 m as obtained from the measured SP anomaly over a graphite ore body, southern Bavarian woods, Germany, using (a) second-derivative method (b), third-derivative method, and (c) fourth-derivative method.

same second-, third-, or fourth-derivative filter as applied to the observed SP data. As a result, this method can be applied not only to residuals but also to observed SP data. The advantage of the present higher derivatives analysis method over our earlier work (Abdelrahman et al., 1997b, 1998) is that it works well in the presence of regional components represented by a polynomial of any order.

We have also developed a method, based on a least-squares minimization approach to determine successively the depth and shape of a buried structure from the residual SP anomaly. The problem of determining the depth and shape from the SP residual anomaly has been transformed into the problem of finding a solution of a nonlinear equation and a linear equation, respectively. The advantage of the present least-squares method over previous least-squares techniques (Abdelrahman and Sharafeldin, 1997; Abdelrahman et al. 1997a) is that each model parameter is computed from all observed data.

Given their relative strength, our methods complement the existing fixed geometry methods of depth and shape determination, and overcome some of their shortcomings. Obtaining these two parameters together is a powerful means to gain geological insight about the subsurface. Synthetic and field studies demonstrate the efficiency of the present inversion techniques.

Finally, in view of the above facts, we envisage the application of these two methods in solving various problems related to potential field data interpretation in the future.

ACKNOWLEDGMENTS

The authors thank the editors and the three capable reviewers for their excellent suggestions and Dr. Randall L. Mackie, Associate Editor, for the thorough review that improved our original manuscripts.

REFERENCES

Abdelrahman, E. M., Riad, S., Refai, E., and Amin, Y., 1985, On the least-squares residual anomaly determination: Geophysics, **50**, 473–480.

Abdelrahman, E. M., and Sharafeldin, S. M., 1997, A least-squares approach to depth determination from residual self-potential anomalies caused by horizontal cylinders and spheres: Geophysics, **62**, 44–48.

Abdelrahman, E. M., El-Araby, T. M., Ammar, A. A., and Hassanein, H. I., 1997a, A least-squares approach to shape determination from self-potential anomalies: Pure Appl. Geophys., **150**, 121–128.

Abdelrahman, E. M., Ammar, A. A., Sharafeldin, S. M., and Hassanein, H. I., 1997b, Shape and depth solutions from numerical horizontal self-potential gradients: Appl. Geophys., **36**, 31–43.

Abdelrahman, E. M., Ammar, A. A., Hassanein H. I., and Hafez, M. A., 1998, Derivative analysis of SP anomalies: Geophysics, **63**, 890–497.

Agarwal, B. N. P., and Lal, T., 1971, Application of rational approximation in calculation of the second derivative of the gravity field: Geophysics, **36**, 571–581.

Bhattacharya, B. B., and Roy, N., 1981, A note on the use of nomograms for self-potential anomalies: Geophys. Pros., **29**, 102–107.

Demidovich, B. P., and Maron, I. A., 1973, Computational mathematics, Mir Publ.

Furness, P., 1992, Modelling spontaneous mineralization potentials with a new integral equation: J. Appl. Geophys., **29**, 143–155.

Guptasarma, D., 1983, Effect of surface polarization on resistivity modelling: Geophysics, **48**, 98–106.

Hammer, S., 1977, Graticule spacing versus depth discrimination in gravity interpretation: Geophysics, **42**, 60–65.

Jackson, D. D., 1972, Interpretation of inaccurate, insufficient and inconsistent data: Geophys. J. Roy. Astr. Soc., **28**, 97–109.

Meiser, P., 1962, A method of quantitative interpretation self-potential measurements: Geophys. Prosp., **10**, 203–218.

Nettleton, L. L., 1976, Gravity and magnetic in oil prospecting: Mc-Graw Hill Book Co.

Paul, M. K., 1965, Direct interpretations of self-potential extension anomalies caused by inclined sheets of infinite horizontal extension: Geophysics, **30**, 418–423.

Peters, L. J., 1949, The direct approach to magnetic interpretation and its practical application: Geophysics, **14**, 290–320.

Rao, A. D., and Babu, R. H. V., 1983, Quantitative interpretation of self-potential anomalies due two-dimensional sheet-like bodies: Geophysics, **48**, 1659–1664.

Shi, W., and Morgan, F. D., 1996, Non-uniqueness in self-potential inversion: 66th Ann. Internat. Mtg., Soc. Expl. Geophys., Extended Abstracts, 950–953.

Stanley, J. M., 1977, Simplified magnetic interpretation of the geologic contact and thin dike: Geophysics, **42**, 1236–1240.

Syberg, F. J. R., 1972, A Fourier method for the regional-residual problem of potential fields: Geophys. Prosp., **20**, 47–75.

Yungul, S., 1950, Interpretation of spontaneous polarization anomalies caused by spherical ore bodies: Geophysics, **15**, 237–246.